THE ASTROPHYSICAL JOURNAL, 444:452–457, 1995 May 1

THE STRUCTURE OF THE DUST SHELLS AROUND IRC +10216[1]

G. C. SLOAN[2] AND M. P. EGAN
Geophysics Directorate, Phillips Laboratory PL/GPOB, 29 Randolph Road, Hanscom AFB, MA 01731-3010;
sloan@ssa1.arc.nasa.gov, egan@pldac.plh.af.mil
Received 1994 June 16; accepted 1994 November 2

ABSTRACT

We have investigated IRC +10216 using a long-slit mid-infrared spectrometer and modeling the circumstellar dust distribution with a radiative transfer algorithm. Maximum entropy reconstructions of the spectral images made with the slit oriented north/south and east/west reveal three components. Two shells of cool carbon-rich dust are seen, as well as a region of blue emission between the shells, ~1″ north of the central source. The dust shell structure agrees well with previous interferometric observations: a circularly symmetric inner shell enclosed within an outer shell elongated roughly north/south. The blue emission appears to arise from a region of small grains of radiatively heated amorphous carbon and implies that the polar regions of the inner shell are optically thinner than the equatorial regions.

Subject headings: circumstellar matter — dust, extinction — stars: individual (IRC +10216)

1. INTRODUCTION

As the brightest source beyond the solar system in the mid-infrared sky, IRC +10216 has received a great deal of attention from astronomers. Soon after the discovery of this carbon-rich Mira in the Two Micron Sky Survey (Neugebauer & Leighton 1969), Toombs et al. (1972) resolved IRC +10216 into a core-halo structure from 2 to 10 μm during a lunar occultation; the core had a FWHM of 0.″4 and was embedded within an extended halo of cooler dust with FWHM 2.″0. High-resolution studies from 2 to 5 μm have revealed that the outer halo is elongated by roughly a factor of 2 (2″ × 4″) along a position angle of 20°–30° (McCarthy, Howell, & Low 1980; Dyck et al. 1987).

IRC +10216 is an extreme carbon star (C9, 5; Cohen 1979), pulsates with a period between 628 and 649 days (Jones et al. 1990; Le Bertre 1992), and is shedding mass at a terminal velocity of 15 km s^{-1} (Knapp 1985). Herbig & Zappala (1970) estimated the distance to IRC +10216 to be ~290 pc, but Zuckerman, Dyck, & Claussen (1986) have argued that it could be as close as 100 pc. The uncertainty in distance has led to a range of estimates of the mass-loss rate. At an assumed distance of 180 pc, most mass-loss estimates scale to $\sim 2 \times 10^{-5}$ $M_\odot$ yr^{-1} (Knapp & Morris 1985; Kastner 1992; Danchi et al. 1994). All of these properties indicate that IRC +10216 is a highly evolved object on the thermal pulsing portion of the asymptotic giant branch (Iben & Renzini 1983; Bedijn 1987, 1988; van der Veen 1988; Jones et al. 1990).

IRC +10126 is moderately polarized perpendicular to the angle of elongation, suggesting that it has begun to evolve toward the axisymmetric geometry characteristic of proto–planetary nebulae such as AFGL 2688 and AFGL 618 (Shawl & Zellner 1970; Kastner & Weintraub 1994). Dyck et al. (1991) discuss additional evidence for deviations from spherical symmetry. Speckle interferometry through the 1980s revealed a shoulder in the spatial profile of IRC +10216 at 2.2 μm, located north of the central source, ~0.″5 away. It appeared in profiles taken from 1982 to 1985, but was missing in subsequent observations in 1988 and 1989.

The proximity of IRC +10216, its evolved state, complicated structure, and the observed changes over the past decade make this object an important candidate for further study. We have chosen to examine IRC +10216 using a long-slit mid-infrared spectrometer and a novel maximum entropy reconstruction algorithm to search for spatial variations in the spectral emission from within the source. This technique has already been used to reveal the double-shell structure of α Ori and changes in grain properties in the outflows of the Red Rectangle (Sloan, Grasdalen, & LeVan 1993a, b). This method, in conjunction with radiative transfer models of the circumstellar dust, can provide further clues to the geometry and evolutionary status of IRC +10216.

2. OBSERVATIONS

We made all observations with the Air Force Geophysics Laboratory 10 μm Array Detector Spectrometer (GLADYS) mounted at the f/27 Cassegrain focus of the 2.3 m reflecting telescope of the Wyoming Infrared Observatory (WIRO). In GLADYS, radiation passes through a 2″ slit and is dispersed by NaCl prism onto a 58 × 62 array of Si:Ga detectors. Each of the 58 rows subtends 0.″9 along the slit. The 62 columns cover wavelengths from 7 to 14 μm; the resolution ($\lambda/\Delta\lambda$) varies from about 100 to 50. More details can be found in LeVan (1990) and Sloan (1992).

We obtained the data in 1993 March, the first observing run for GLADYS since a complete upgrade of the electronics. We replaced the detector drive electronics, the analog-to-digital converters, and the hardware co-adder with new electronics from Wallace Instruments. In its new configuration, GLADYS reads each pixel in 3.3 μs; to read the entire array takes 5.9 ms. We chopped the secondary at a frequency of 2.5 Hz to correct for and remove the background, using the three-beam chop described by Landau, Grasdalen, & Sloan (1992). A typical image written to disk contains 5140 individual reads of the array on-source and 5140 off-source, for a total integration

[1] Contribution 144 of the Wyoming Infrared Observatory.
[2] Current address: NASA Ames Research Center, MS 245-6, Moffett Field, CA 94035-1000.

time of 30 s in each beam position. We integrated on IRC +10216 with the slit north/south for 150 s on 1993 March 1 and for 300 s the following night with the slit east/west.

3. DATA REDUCTION

The exposure time for each pixel has increased substantially with the new electronics, revealing the nonlinear character of the response functions of the pixels. For IRC +10216, which is as bright as the background radiation, nonlinearities become even more significant. We obtained flat-fielding data as before (Sloan et al. 1993a). To model the changes in responsivity with incident flux, we check each pixel against its neighbors over a range of fluxes.

We used a maximum entropy reconstruction algorithm developed for long-slit mid-infrared spectroscopy (Sloan et al. 1993a; Sloan & Grasdalen 1995) to deconvolve the point-spread function (PSF) from the flat-fielded images. The key step in the algorithm is the construction of a PSF for each wavelength observed, which requires careful monitoring of a point-source standard. Because a separate PSF must be constructed at each wavelength and because the wings of the PSF must be known accurately, the standard must be bright.

For the north/south slit, we made reconstructions using three different PSFs, two from separate integrations of α Boo and one with the fainter standard μ UMa. All were qualitatively consistent, despite the limited quality of the PSF constructed from μ UMa. For the east/west slit, we attempted to construct PSFs from images of α CMi and μ UMa, but the S/N in the wings of the PSF proved inadequate. As a consequence, we were forced to use a PSF based on observations made the same night of α Boo, but in a north/south slit orientation. To correct for the differences between the PSF in the north/south and east/west slits, we used observations of μ Cep made with the slit in both positions on a subsequent night. Other observations with GLADYS (1991 February 11 and 1993 June 28) showed no evidence that μ Cep was spatially extended from 7 to 14 μm either north/south or east/west and could therefore serve as a spatial standard. Using μ Cep resulted in a good PSF and reasonable reconstructions. Nonetheless, the east/west data should be treated as less certain than the north/south reconstructions.

In all, we reconstructed five individual images in the north/south slit and 10 images in the east/west slit; these were averaged into two final reconstructed images, illustrated in Figure 1 (Plate 14). The reconstruction algorithm regridded the data to a smaller pixel size, 0".45 pixel^{-1}. The width of the pixels across the slit is still 2".0 in the reconstructions.

All spectra extracted from our reconstructions are corrected for atmospheric and instrumental transmission. We determined the transmission by dividing the observed spectrum by its assumed intrinsic spectrum. For the north/south data, β Gem (K0 IIIb) served as a spectroscopic standard; for the east/west data, we used μ UMa (M0 III) and α CMi (F5 IV). We assumed each spectrum could be modeled by an Engelke function (Engelke 1992). We modeled β Gem with an effective temperature of 4400 K and flux at 7.7 μm of 206 Jy. For α CMi, the effective temperature was 6600 K, and the 7.7 μm flux was 133 Jy. We took the effective temperature of μ UMa to be 3300 K and the 7.7 μm flux to be 175 Jy. To account for the SiO absorption in this source, we used the spectrum from the *IRAS* Low-Resolution Spectrometer (LRS) from 7.7 to 11.1 μm (*IRAS* Science Team 1986) obtained from the University of Calgary database and corrected as described by Cohen, Walker, & Witteborn (1992).

4. RESULTS AND DISCUSSION

4.1. *Structure of the Dust Shells*

Our reconstructions reveal three components to the structure of IRC +10216 in the mid-infrared: a circularly symmetric inner shell, an elongated outer shell, and an unexpected region of blue emission between the two shells, $\sim$1" north of the central source. Figure 2 shows the spatial profiles in both slit positions, and Figure 3 illustrates the spectra of the three different components.

The inner shell is represented in both reconstructions by rows 9–11. Fitting a Gaussian to the spatial profile in these rows gives a FWHM of 0".69 $\pm$ 0".04 east/west and 0".73 $\pm$ 0".07 north/south. On the basis of these numbers, the shell appears to be circularly symmetric with a FWHM of 0".7. Rows 9–11 from the two slit positions completely overlap each other, so the inner shell spectrum in Figure 3 represents the average of the spectrum for each reconstruction (produced by summing rows 9–11).

The outer shell is represented in the east/west reconstruction by rows 5–8 (the east limb) and rows 12–15 (the west limb) and in the north/south reconstruction by rows 4–8 (the south limb) and rows 14–15 (the north limb). Because these rows do not overlap significantly in the two reconstructions, we simply sum

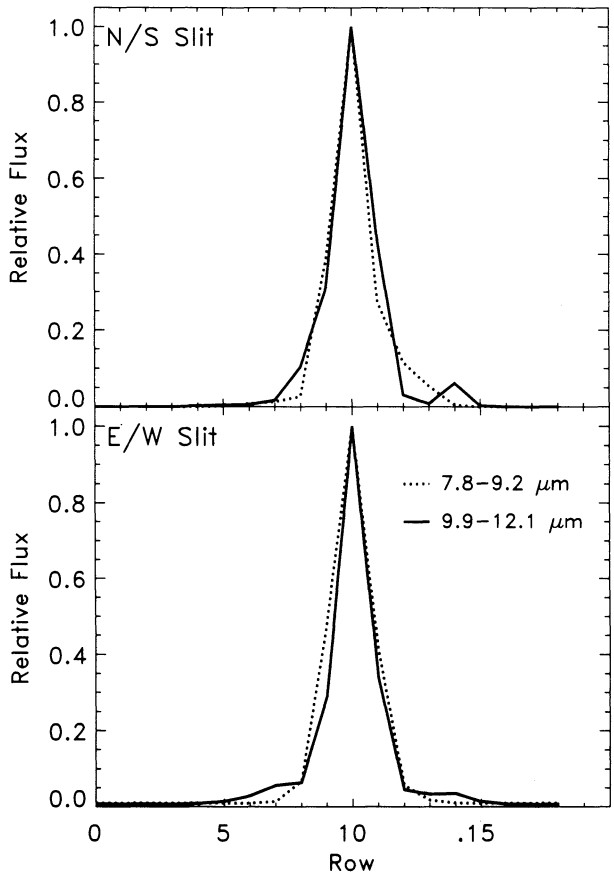

FIG. 2.—Spatial profiles of IRC +10216 north/south (*top*) and east/west (*bottom*) after reconstruction. The dotted line represents emission over the wavelength range 7.8–9.2 μm; the dashed line represents 9.9–12.1 μm.

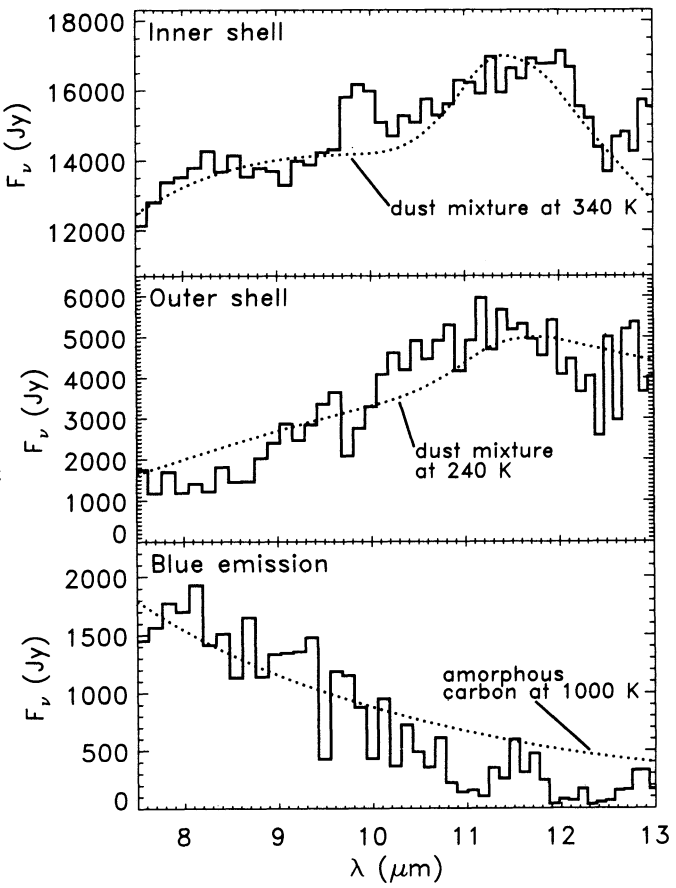

FIG. 3.—Spectra of the three regions seen in the reconstructions. *Top*: Inner shell, averaged from the central three rows in the north/south and east/west slit. The bump at 9.7 μm is an artifact which results from a poor PSF in the telluric ozone absorption feature. A dust mixture of 90% amorphous carbon and 10% SiC radiating at 340 K matches the spectrum well. *Center*: Outer shell, the sum of rows 4–8 and 14–15 north/south and rows 5–8 and 12–15 east/west. The spectrum can be matched with the same dust mixture used for the inner shell, but radiating at 240 K. Note the slight trough at 9.7 μm corresponding to the emission artifact in the inner shell. *Bottom*: Blue emission, the sum of rows 12 and 13 in the north/south reconstruction. The spectrum can be matched roughly with amorphous carbon radiating at 1000 K.

all of these rows to produce the spectrum in Figure 3. Most of the emission in the limbs to the east, west, and south occurs ~1″ away from the central source, but the north limb is both fainter and further away. We interpret this asymmetry as a sign of the elongation of the outer halo in the north/south direction detected by McCarthy et al. (1980).

4.2. *Radiative Transfer Models*

We can aid our interpretation of the reconstructions by developing radiative transfer models of the dust around IRC +10216. These models must be constrained by the photometric observations (Gezari, Schmitz, & Mead 1987; LeBertre 1992), the LRS spectrum, and the physics of circumstellar mass loss and dust formation. Using the quasi-diffusion method of Leung (1975, 1976) as implemented in the CSDUST3 code (Egan, Leung, & Spagna 1988), we have constructed spherically symmetric radiative transfer models in an effort to match the LRS spectrum and spectral energy distribution (SED) of IRC +10216.

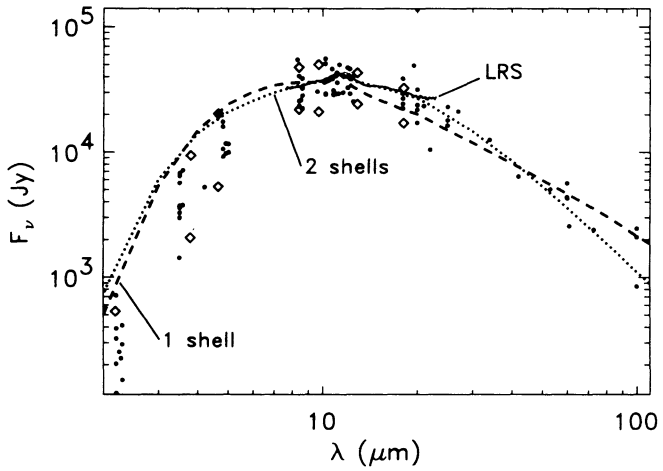

FIG. 4.—Results of the radiative transfer models. The photometric data from Gezari et al. (1987) are plotted with dots. The diamonds represent the minima and maxima from the observations of LeBertre (1992). The solid line is the LRS spectrum. The two-shell model (*dotted line*) fits the observed data much better than the one-shell model (*dashed line*).

Most previous modeling efforts have concentrated on fitting the SED (Martin & Rogers 1987; Lorentz-Martins & Lefevre 1993). Griffin (1990) attempted to fit the SED and the spectrum from the LRS simultaneously in order to more tightly constrain the resulting model parameters. Unfortunately, the LRS database is affected by the SiO absorption in the standard star α Tau (Cohen et al. 1992). Correcting for this results in an 8% drop in the spectral emission at 8 μm and makes Griffin's model bluer than the LRS (see Fig. 5). In general, these models determine that the opacity of the circumstellar dust must be ~1 at 11 μm. Griffin (1990) finds that using smaller grains (0.005–0.05 μm) than the standard model of Mathis, Rumpl, & Nordsieck (1977; 0.005–0.25 μm) improves the fit to the SED. All models require only a relatively low SiC abundance.

The CSDUST3 code treats the stellar temperature, luminosity, and radius as inputs for the heating source. We have assumed that IRC +10216 was at a phase of 0.1 when the LRS data were obtained and that the effective temperature was 2460 K, the angular radius 0.″0218, and the distance 180 pc. We also assumed that the dust was a mixture of 90% amorphous

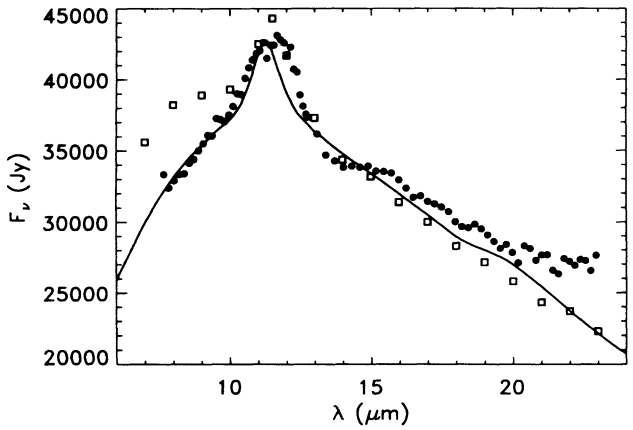

FIG. 5.—Two-shell model (*solid line*), compared to the corrected LRS (*filled circles*). We have extracted data from Griffin's best-fitting model (1990, Fig. 11) and plotted these as rectangles.

carbon and 10% SiC, using the constants of Mathis & Whiffen (1989) and Pegourie (1988), respectively. This SiC abundance is higher than used before (e.g., 6% SiC; Griffin 1990), but is necessary to match the shape of the 11.3 μm SiC feature in the LRS spectrum. Given the uncertainties in the radiative properties of SiC, this difference is slight. For simplicity, our models use a single grain size of 0.01 μm radius. Our goal was to determine the morphology of the circumstellar dust necessary to fit the SED and LRS by varying the boundaries of the inner and outer shells.

Figures 4 and 5 illustrate the results of attempts to fit our models to the observed data. While a single-shell model can approximate the SED, we were unable to produce a model which also fit the corrected LRS. Like Griffin's model, our best single-shell fit to the SED is too blue for the LRS. Improving the fit to the LRS by extending the shell to produce more cool dust degrades the fit to the SED. We can decrease the proportion of warm dust by changing the power law of the density distribution. However, in order to fit the SED and the LRS, we find that the density must fall as $r^{-1.2}$ throughout the entire shell and the opacity at 11 μm (τ_{11}) must be reduced to 0.7. While there is evidence for an $r^{-1.5}$ power law in the dust acceleration zone (Danchi et al. 1994), a power law of 1.2 over the entire shell is physically unrealistic. Using a double-shell model, we can fit both the SED and LRS while maintaining the inverse square density distribution and a reasonable opacity. Table 1 provides the details of our models.

The infrared emission from the inner shell in the model can be roughly fit with a Gaussian with a FWHM of 0".5, a good approximation of the interferometric results from the early 1980s. The results from the radiative transfer models, the reconstructions of the long-slit spectroscopy, and previous interferometric measurements all support one another. We can state with confidence that the central star of IRC +10216 is embedded within two dust shells emitting strongly in the infrared. Thus, IRC +10216 is not losing mass at a steady rate. If we assume that the dust is moving outward at a constant rate of 15 km s^{-1} and that IRC +10216 is 180 pc away, then extrapolating back in time leads to the conclusion that, from about 1900 to 1940, the mass-loss rate was strongly diminished. Submicron images by Crabtree, McLaren, & Christian (1987) also show discrete shells at further distances, 15"–30", indicating that the mass-loss rate has been varying for at least the past two centuries.

An expansion rate of 15 km s^{-1} implies that the inner shell is expanding at a rate of $\sim$0".2 per decade. That would explain why the inner shell is somewhat larger in our spectral reconstructions than in previous work or in our radiative transfer models (which are based on data from earlier epochs). We should emphasize, however, that a difference of 0".2 between our reconstructions and other work could possibly result from differences in the data acquisition and reduction techniques. Further observations could resolve this issue.

TABLE 1

RESULTS OF RADIATIVE TRANSFER MODELS

Model	τ_{11}	θ_{in}	θ_{out}
One shell, $n \sim r^{-2.0}$.....	1.3	0".087	190"
Two shells, $n \sim r^{-2.0}$:			
Inner shell.....	1.1	0.055	0.67
Outer shell	0.14	1.5	5.2

4.3. *The Blue Emission*

In addition to the two shells, we have also observed a third component, the blue spectrum seen on rows 12 and 13 in the north/south slit. It does not appear in the east/west slit. This position corresponds to a region between the two shells, $\sim$ 0".9–1".5 north of the central star. The quality of the reconstructions of the dust shells makes it difficult to explain the blue emission as an artifact of the reconstruction method. We have ruled out asymmetries in the PSF as a possible cause. A misalignment between the dispersion axis of the prism and the row axis of the detector array could also produce an artifact of this nature, but our reconstructions correct for this.

As discussed by Sloan & Grasdalen (1995), the reconstruction algorithm may shift the position of a side-row spectrum by a row or so in the reconstructed image. Thus, it is possible that the blue emission could arise from a position as close as 0".5 from the central source. At this distance, amorphous carbon grains in equilibrium with the stellar radiation field would be heated to over 900 K if they had a size of 0.1 μm (larger or smaller grains would be slightly cooler). As shown in Figure 3, amorphous carbon radiating at 1000 K or so might produce the observed spectrum. Because the maximum entropy algorithm reconstructs each column (wavelength) independently of the others, one must be careful not to overinterpret the point-to-point variations in the spectra on each row. For this reason, we believe that radiative heating of amorphous carbon dust is consistent with the blue emission spectra seen on rows 12 and 13 of the north/south reconstruction, despite the imperfect match between the actual data and the theoretical spectrum.

We have also investigated and ruled out a number of other possibilities. The blue emission does not appear to result from scattering, primarily because there is simply not enough stellar flux at 8 μm to scatter. Even if there were, we would expect the thermal emission from the grains to dominate the scattering component. Note that these arguments do not apply to measurements in the near-infrared, where scattering may be responsible for the structure observed at 2 μm north of the central source during the 1980s. Collisional heating of a high-velocity clump of material also seems unlikely. At the expected densities around IRC +10216 ($\sim 10^{-17}$ g cm^{-3} at 1") even a particle traveling 300 km s^{-1} would only be heated to $\sim$200 K. Fluorescent emission from small grains is another possibility, but this mechanism would require more UV radiation from the central source than is presently believed to exist.

Dyck et al. (1991) raised the possibility that an orbital companion might be responsible for the transient shoulder in the spatial profile of IRC +10216 seen at 2.2 μm. If the blue emission we have observed arises from the same source, then it would be orbiting IRC +10216 with a period of $\sim$10 yr. The separation between the blue emission and the central source must be at least 0".5. If we assume a distance of 180 pc, then the semimajor axis would be at least 90 AU, implying a system mass of over 7000 $M_\odot$, much too excessive to be plausible.

4.4. *The Geometry of IRC +10216*

Whatever the specific origin of the blue emission, it indicates that the dust distribution in the inner shell is asymmetric. The 2.2 μm shoulder north of the central source discussed by Dyck et al. (1991) and the moderate polarization of IRC +10216 in the near-infrared (Kastner & Weintraub 1994) provide further evidence for departures from spherical symmetry.

On the other hand, our radiative transfer model *can* match the SED and LRS data using spherically symmetric shells,

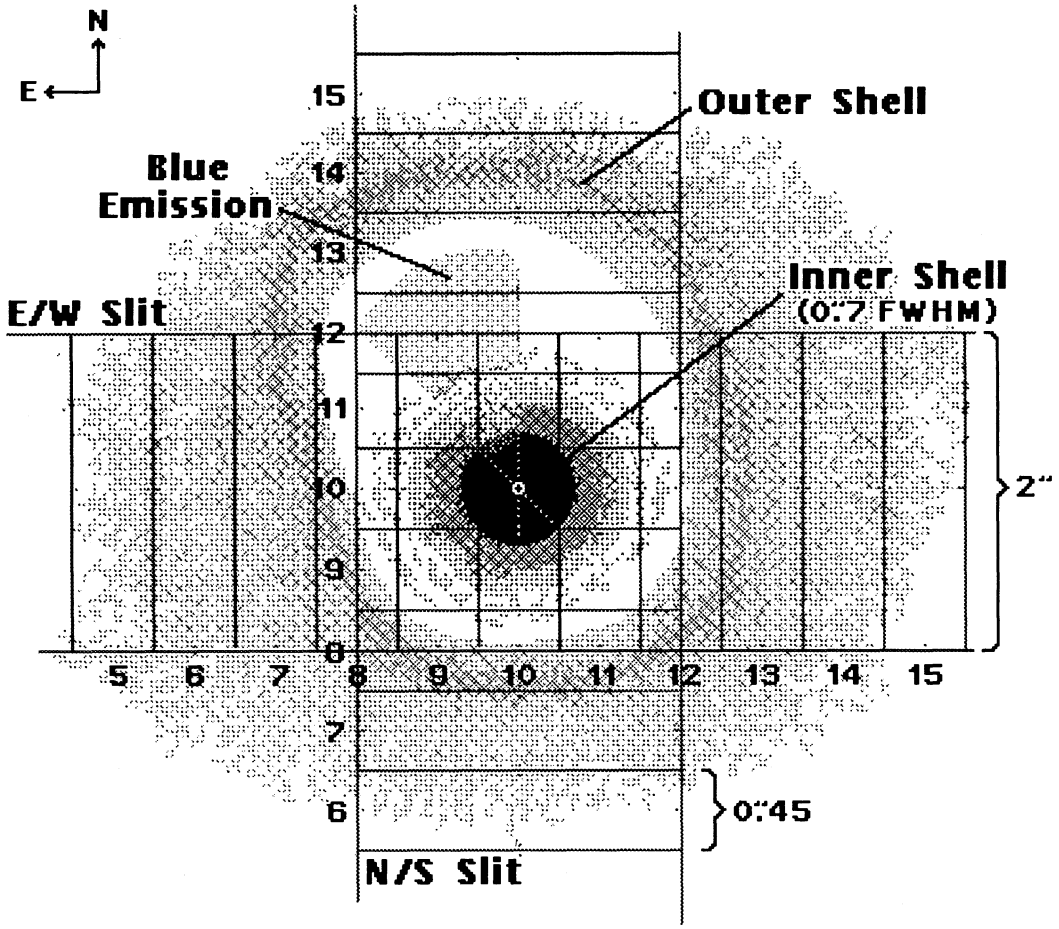

FIG. 6.—One possible scenario for the geometry of IRC +10216, with the spectrometer slit drawn for both the east/west and north/south slit positions. Each slit is 2″ across, and in the reconstructed images, the spacing between adjacent rows is 0″.45. So each 0″.45 × 2″ rectangle in this picture produces the spectrum from one row of the reconstructed spectral images in Fig. 1. Of note are the elongated outer shell, the inner shell which is nearly circularly symmetric, and the blue emission seen in rows 12 and 13 in the north/south reconstruction. The specific shape of the blue emission within rows 12 and 13 and the deviations from circular symmetry in the inner shell are somewhat conjectural.

implying that the asphericities in the inner shell are not large enough to dominate the total emission. Previous investigators have suggested that the innermost dust may have a disklike distribution, but a disk represents a radical departure from spherical symmetry. We suggest that the inner shell could be better described as a nearly spherical shell, but with evacuated poles. Such a geometry is consistent with our radiative transfer models, the blue emission we have observed, the 2 μm shoulder, and the moderate degree of polarization. Figure 6 depicts a possible scenario for the geometry we envision.

Yusef-Zadeh, Morris, & White (1984) have used a similar geometry to model the optical appearance of bipolar proto–planetary nebulae such as the Cygnus Egg (AFGL 2688). The Egg probably represents the next phase in the evolution of IRC +10216 (e.g., Zuckerman et al. 1976). Despite the clear axisymmetric appearance of the Egg in the optical and near-infrared (Ney et al. 1975; Latter et al. 1993), it is nearly symmetric at 10 μm (Jaye et al. 1989; Sloan et al. 1993c). We are viewing the Egg nearly edge-on, so its mid-infrared appearance, while incompatible with a disklike structure, is suggestive of a dust shell with evacuated poles. The similarity to IRC +10216 is remarkable.

Johnson & Jones (1991) searched for polarization in a sample of sources representing each stage in the development of planetary nebulae and found that asymmetric dust distributions were common even on the asymptotic giant branch. The polarizations they measured were only on the order of a few percent, making highly flattened disklike structures unlikely. Therefore, the dust geometry of IRC +10216 is probably typical.

If circumstellar dust shells with evacuated poles represent the rule rather than the exception, it is important to understand how this geometry is produced. The answer may lie in the discussion by Salpeter (1974), who suggested that the photospheres of evolved stars may have patchy temperature distributions. Dust would form more readily over the cooler patches. If these patches tend to occur at lower stellar latitudes (e.g., if they were starspots), then as a star sheds its envelope, dust would form sooner and accumulate over the equatorial regions of the star. There are many other possibilities. Perhaps the mass loss itself or the outflow velocity are functions of stellar latitude. One fact is growing clearer: circumstellar dust shells are not spherically symmetric.

We would like to thank R. Canterna for the use of computing facilities to generate the reconstructions. P. Tandy and B.

Pirger were vital to the refurbishment of GLADYS, and T. Hodge assisted with observations at WIRO. We found the LRS database at the University of Calgary extremely helpful. Many stimulating conversations have helped shape this paper, in particular, we thank H. M. Dyck and R. Shipman. The suggestions of our referee led to many improvements in the manuscript. For the duration of this work G. C. S. was supported by the Phillips Laboratory Scholar program, and GLADYS was maintained by the US Air Force.

REFERENCES

Bedijn, P. J. 1987, A&A, 186, 136
———. 1988, A&A, 205, 105
Cohen, M. 1979, MNRAS, 186, 837
Cohen, M., Walker, R. G., & Witteborn, F. C. 1992, AJ, 104, 2030
Crabtree, D. R., McLaren, R. A., & Christian, C. A. 1987, in Late Stages of Stellar Evolution, ed. S. Kwok & S. R. Pottasch (Dordrecht: Reidel), 145
Danchi, W. C., Bester, M., Degiacomi, C. G., Greenhill, L. J., & Townes, C. H. 1994, AJ, 107, 1469
Dyck, H. M., Benson, J. A., Howell, R. R., Joyce, R. R., & Leinert, Ch. 1991, AJ, 102, 200
Dyck, H. M., Zuckerman, B., Howell, R. R., & Beckwith, S. 1987, PASP, 99, 99
Egan, M. P., Leung, C. M., & Spagna, G. F. 1988, Comput. Phys. Comm., 48, 271
Engelke, C. W. 1992, AJ, 104, 1248
Gezari, D. Y., Schmitz, M., & Mead, J. M. 1987, Catalog of Infrared Observations (NASA RP-1196) (Washington, DC: GPO)
Griffin, I. P. 1990, MNRAS, 247, 591
Herbig, G. H., & Zappala, R. R. 1970, ApJ, 162, L15
Iben, I., & Renzini, A. 1983, ARA&A, 21, 271
IRAS Science Team. 1986, A&AS, 65, 607
Jaye, D., Tresch Fienberg, R., Fazio, G. G., Gezari, D. Y., Hoffmann, W. F., Lamb, G. M., Shu, P. K., & McCreight, C. R. 1989, AJ, 97, 809
Johnson, J. J., & Jones, T. J. 1991, AJ, 101, 1735
Jones, T. J., Bryja, C. O., Gehrz, R. D., Harrison, T. E., Johnson, J. J., Klebe, D. I., & Lawrence, G. F. 1990, ApJS, 74, 785
Kastner, J. H. 1992, ApJ, 401, 337
Kastner, J. H., & Weintraub, D. A. 1994, ApJ, 434, 719
Knapp, G. R. 1985, ApJ, 293, 273
Knapp, G. R., & Morris, M. 1985, ApJ, 292, 640
Landau, R., Grasdalen, G., & Sloan, G. C. 1992, A&A, 259, 696
Latter, W. B., Hora, J. L., Kelly, D. M., Deutsch, L. K., & Maloney, P. R. 1993, AJ, 106, 260
Le Bertre, T. 1992, A&AS, 94, 377
Leung, C. M. 1975, ApJ, 199, 340
———. 1976, J. Quant. Spectrosc. Rad. Transf., 16, 599
LeVan, P. D. 1990, PASP, 102, 190
Lorenz-Martins, S., & Lefevre, J. 1993, A&A, 280, 567
Martin, P. G., & Rogers, C. 1987, ApJ, 322, 374
Mathis, J. S., Rumpl, W., & Nordsieck, K. H. 1977, ApJ, 217, 425
Mathis, J. S., & Whiffen, G. 1989, ApJ, 341, 808
McCarthy, D. W., Howell, R., & Low, F. J. 1980, ApJ, 235, L27
Neugebauer, G., & Leighton, R. B. 1969, Two Micron Sky Survey—A Preliminary Catalog (NASA SP-3047) (Washington, DC: GPO)
Ney, E. P., Merrill, K. M., Becklin, E. E., Neugebauer, G., & Wynn-Williams, C. G. 1975, ApJ, 198, L129
Pegourie, B. 1988, A&A, 194, 335
Salpeter, E. E. 1974, ApJ, 193, 585
Shawl, S. J., & Zellner, B. 1970, ApJ, 162, L19
Sloan, G. C. 1992, Ph.D. thesis, Univ. Wyoming
Sloan, G. C., & Grasdalen, G. L. 1995, A&A, submitted
Sloan, G. C., Grasdalen, G. L., & LeVan, P. D. 1993a, ApJ, 404, 328
———. 1993b, ApJ, 409, 412
Sloan, G. C., Tandy, P. C., Pirger, B. E., & Hodge, T. M. 1993c, BAAS, 25, 876
Toombs, R. I., Becklin, E. E., Frogel, J. A., Law, S. K., Porter, F. C., & Westphal, J. A. 1972, ApJ, 173, L71
van der Veen, W. 1988, Ph.D. thesis, Univ. Leiden
Yusef-Zadeh, F., Morris, M., & White, R. L. 1984, ApJ, 278, 186
Zuckerman, B., Dyck, H. M., & Claussen, M. J. 1986, ApJ, 304, 401
Zuckerman, B., Gilra, D. P., Turner, B. E., Morris, M., & Palmer, P. 1976, ApJ, 205, L15

PLATE 14

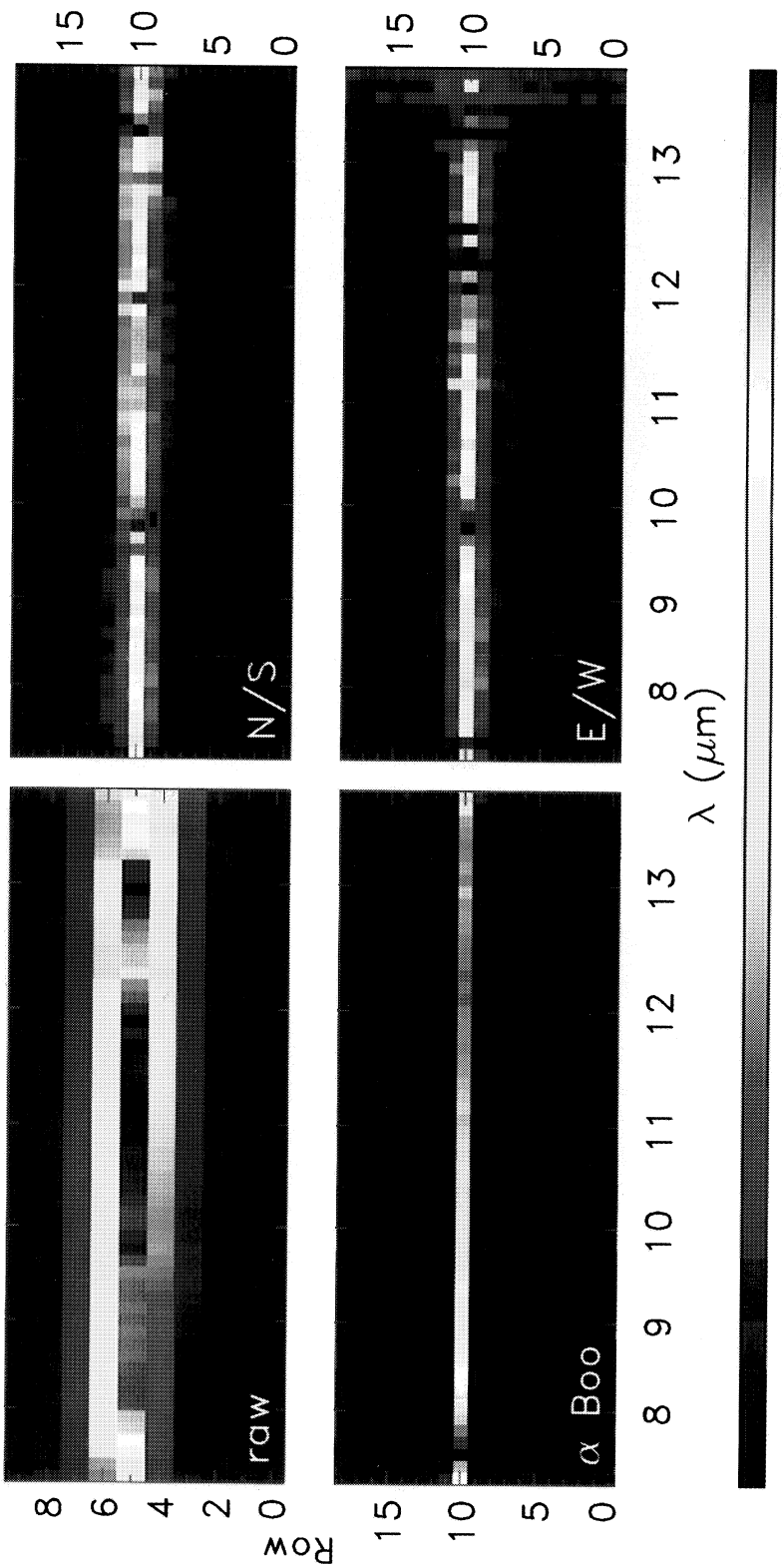

FIG. 1.—Four GLADYS images, before and after maximum entropy reconstruction. In each image, each row represents a spectrum from a different portion of the slit. The horizontal axis is the spectral direction. Each image covers a 2″ × 9″ field of view (slit width of 2″, spatial extent of 9″) and has been flat-fielded and corrected for atmospheric and instrumental transmission. *Upper left*: A 10-row portion of one image of IRC +10216 (north/south) before reconstruction. The reconstruction algorithm will map these 10 rows (each subtending 0.″9) into 19 rows (0.″45 each). *Lower left*: Reconstruction of α Boo, an unresolved source used as a point-source standard. The maximum entropy algorithm has placed almost all of the flux onto the central row, row 10. *Upper right*: Average of all reconstructions of IRC +10216 in the north/south slit. The central three rows (9–11) correspond to the inner shell; rows 4–8 and 14–15 correspond to the outer shell. Rows 12 and 13 contain the unexpected blue emission (i.e., ~0.″9–1.″4 north of the center). *Lower right*: Average of all reconstructions of IRC +10216 in the east/west slit. The inner shell occupies rows 9–11; the flux outside of these rows corresponds to the outer shell. No blue emission is apparent. Peak fluxes (in Jy arcsec^{-2}) are: upper left, 10,200; lower left, 1160; upper right, 13,400, lower right, 16,100.

SLOAN & EGAN (see 444, 453)